Materials Horizons

ROYAL SOCIETY OF CHEMISTRY

COMMUNICATION

View Article Online
View Journal | View Issue

Cite this: *Mater. Horiz.*, 2022, 9, 2893

Received 22nd May 2022,
Accepted 31st August 2022

DOI: 10.1039/d2mh00635a

rsc.li/materials-horizons

High energy density primary cathode with a mixed electron/ion interface†

Jingchi Gao,[ab] Feng He,[a] Changshui Huang,*[ab] Yurui Xue,[c] Zicheng Zuo[a] and Yuliang Li*[ab]

An effective and original strategy described as two-dimensional encapsulation is designed to prepare a high-performance fluorinated carbon cathode composed of a fluorinated carbon/graphdiyne heterostructure (CF_x/GDY). The GDY layers of CF_x/GDY strengthened the three-dimensional contacts between the CF_x particles and additive, achieving outstanding charge transport kinetics and accelerating the lithium-ion diffusion dynamic behavior. The obtained electrodes exhibited a significantly enhanced voltage platform of ~2.5 V, improved battery rate performance (5C, 621.6 mA h g^{-1}) and energy density with 2039.3 W h kg^{-1}. The excellent storage kinetics can be ascribed to the electronic structure modulation of fluorinated carbon from GDY, and the hierarchical porosity of GDY to create an effective, stable electron transfer and robust ion transportation. Our results demonstrated that two-dimensional GDY encapsulation has enormous potential in improving the performance of lithium primary batteries.

New concepts

For the purpose of resolving the inferior rate performance of CF_x, we proposed a valid chemical strategy to establish graphdiyne (GDY) encapsulating CF_x with excellent selective and conductivity. Different to existing methods, the two-dimensional (2D) encapsulation method with GDY creates robust and enhanced three-dimensional (3D) contacts between CF_x and the additive. We found that a predominant electronic modulation with a distinct charge distribution and variable intrinsic bandgap was realized, which was demonstrated by theoretical calculation. In addition, this strategy could achieve facile and convenient ion diffusion and electronic transfer for the unique porous and conjugated 2D structure of GDY, creating outstanding dynamic behaviors. Thus, the CF_x/GDY hybrids exhibited diminishable voltage decay in the initial stage of cycling, weaker voltage polarization and an advantageous electrochemistry performance on account of their superior conductivity and robust 3D ion transportation. As confirmed by the morphology and composition upon cycling, the strategy altered the interfacial characteristic between the electrode and electrolyte, and blocked direct contact between them, making the close contact unbroken upon cycling. The degradation of electrolyte is effectively inhibited and the discharge product LiF on the externality is negligible. From the perspective of electronic structure modulation and interfacial design, this GDY encapsulation is further verified as an effective protocol to design remarkable-performance electrode materials.

Introduction

Advanced cathode materials with a high energy density and excellent security are in urgent demand for energy storage fields. Among the conversion-type cathodes employed in the lithium primary battery (LPB) system with enormous success in various specific application fields, such as portable electronics equipment, mini-medical electronics and military devices,[1–4] CF_x cathode shows outstanding electrochemistry performance in terms of theoretical gravimetric energy density of 3725 W h kg^{-1} and volumetric energy density of 9313 W h L^{-1}[5,6] under an extremely wide temperature range from −40 °C to 170 °C. Remarkably, the shell has a significant lifetime of more than ten years and a weaker self-discharge ability below 10%.[7,8] However, some important scientific issues still need to be addressed. CF_x exhibits a severe voltage delay, inferior rate performance and fewer active materials utilization on account of the low electronic conductivity with intrinsically critical kinetics issues.[9–11] Besides, the insulated discharge product LiF on the surface of the cathode would suppress a consecutive lithium-ion diffusion into the bulk structure and so an effective charge transfer. The concerning issues hinder the successful commercialization of Li/CF_x batteries to a great extent.

[a] *Beijing National Laboratory for Molecular Sciences (BNLMS), CAS Research/Education Centre for Excellence in Molecular Sciences, Institute of Chemistry Chinese Academy of Sciences, Beijing, 100190, P. R. China. E-mail: huangcs@iccas.ac.cn, ylli@iccas.ac.cn*

[b] *University of Chinese Academy of Sciences, Beijing, 100049, People's Republic of China*

[c] *Science Centre for Material Creation and Energy Conversion, School of Chemistry and Chemical Engineering, Institute of Frontier and Interdisciplinary Science, Shandong University Jinan, 250100, P. R. China*

† Electronic supplementary information (ESI) available. See DOI: https://doi.org/10.1039/d2mh00635a

For optimizing the performance of Li/CF_x batteries, many researchers have employed appropriate strategies, such as to modify CF_x with organic (PVDF,[12] polypyrrole,[13] and PEDOT[14]) or inorganic components ($Ag_2V_4O_{11}$[15] and MnO_2[16]) to address these issues. In fact, reported literature could effectively improve the extrinsic electronic conductivity of electrodes to some extent, thus boosting the rate capability and specific capacity. However, previous methods somewhat ameliorate the conductivity and sacrifice the lithium ion and electron transfer channel. More meaningful, modulating the electronic structure is an effective strategy to motivate the performance of the electrode and overcome these issues. It remains a challenge to simultaneously meet the demand of adjusting the electronic structure and ensuring two-dimensional encapsulation.

Graphdiyne (GDY) has attracted much attention from scientists since it was successfully fabricated in 2010.[17] In contrast to dominant carbon materials such as graphene and carbon nanotubes with sp^2 hybrids synthesized at a high temperature, a 2D model GDY with an abundant pore structure, large conjugated structure, excellent semiconductor properties and chemical stability could be synthesized under mild conditions.[18–24] These outstanding features are of benefit to achieve a 3D Li^+ transfer and ensure close contacts between active materials, making it a possibility to achieve two-dimensional encapsulation. Theoretical research showed that GDY, with sp/sp^2 hybrids and triangular cavities in the 2D plane, the intrinsic natural characteristics of an uneven charge distribution, and a strengthened electron mobility and conductive network with an adjustable pore structure, could realize an effective charge transfer between GDY and CF_x, therefore modulating the electronic structure of CF_x.[25–31] As a consequence, the superiority of GDY makes it overcome the insulation character and interfacial contact issues of the CF_x cathode owing to its incomparable merits in electronic structure modulation, 3D ion transportation and moderate fabrication.

Herein, we implement a novel two-dimensional encapsulation of CF_x with a sufficient electronic structure modulation to improve the electrochemistry performance of the CF_x cathode. Our research demonstrates that the two-dimensional encapsulated CF_x/GDY hybrids display a high specific capacity and superior rate performance. The two-dimensional encapsulation ensures an efficient and enhanced connectivity between the active materials and conductive media, provides a stable 3D network channel for ion migration and also a rapid electronic transfer. The charge distribution and energy gap of CF_x/GDY hybrids are significantly distinct from those of CF_x, indicating an effective electronic structure modulation, leading to a reduced initial voltage delay, accelerated kinetic behaviours and an outstanding electronic conductivity. The encapsulation could alter the electrode interface to improve the structure and interface stabilities between the cathode and electrolyte, significantly making a close contact upon cycling and the reducing charge mass transfer resistance. In addition, the encapsulation could effectively inhabit particle accumulation of LiF on the surface, of benefit to the diffusion of lithium ions into the bulk structure.

Results and discussion

We successfully achieved a two-step strategy to cover CF_x particles on Cu foil to produce a film with a thickness of about 15 μm (Fig. S1, ESI†) on which ultrathin GDY was grown. The preparation process of related CF_x/GDY hybrids electrode is shown in Fig. 1a. In apparent contrast to individual CF_x particles with a free stacking manner and a relative random size distribution from several hundred nanometres to microns (Fig. 1b and Fig. S2a, ESI†), every CF_x particle encapsulated by ultrathin GDY nano-walls (~4 nm) with a high tap density formed a 3D hierarchical porous structure, which was of benefit to electronic and ion transfer (Fig. 1e, Fig. S2b and S3, ESI†).[19,25] As shown in Fig. 1c and d, it was obviously that CF_x presented a sheet-like structure and the corresponding high-resolution TEM (HRTEM) image displayed no lattice fringes, indicated in an amorphous structure in essence. The TEM image (Fig. 1f) reveals the morphology of CF_x/GDY hybrids. We could clearly observe the close interface between the CF_x particles and GDY nano-walls, forming massive area contacts (Fig. 1g). The interlayer distance at the edge is about 0.365 nm, corresponding to the well-defined layered structure of GDY. The results demonstrate that CF_x encapsulated by GDY is retained in the two-dimensional mode. Energy dispersive mapping (EDS) results of CF_x (Fig. S4a, ESI†) demonstrated the uniform distribution of elements C and F before (Fig. S4a, ESI†) and after (Fig. S4b, ESI†) the encapsulation of GDY nano-walls. We found fewer F and more C elements on the externality of two-dimensional encapsulation CF_x/GDY hybrids (Fig. S4b, ESI†).

Based on the Raman results in Fig. 2a, we could come to the conclusion that the CF_x/GDY hybrids were fabricated successfully through two-dimensional layered encapsulation due to the emergence of a sharp peak at 2186 cm^{-1} (C≡C).[32,33]

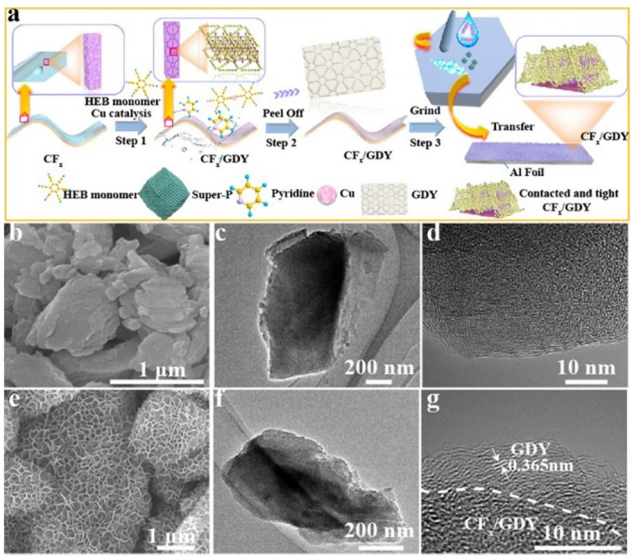

Fig. 1 (a) Schematic illustration of the synthesis of CF_x/GDY. High-resolution SEM images of CF_x (b) and CF_x/GDY (e). TEM images (c and f) and HRTEM images (d and g) of CF_x and CF_x/GDY, respectively.

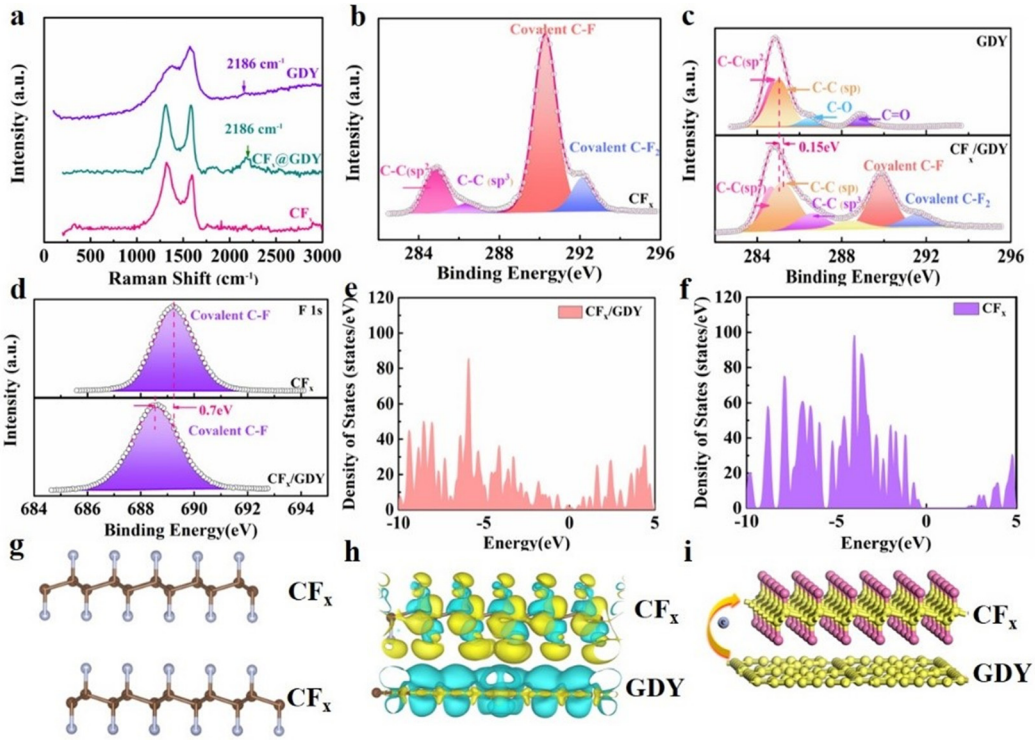

Fig. 2 Raman spectra (a) from pristine CF_x, GDY and CF_x/GDY. C 1s and F 1s spectra of CF_x (b and d), GDY (c) and CF_x/GDY (c and d). Total densities of states of CF_x (e) and CF_x/GDY (f) and the corresponding electron density differences (g and h), respectively, and the corresponding schematic diagram (i).

Fourier transform infrared spectroscopy (FTIR) was applied to check the existence of GDY. The obvious peaks at 1450 and 1587 cm^{-1} (skeletal vibrations of the aromatic ring) and 2110 cm^{-1} (vibrations of the conjugated C≡C bonds) in the spectra of the CF_x/GDY hybrids (Fig. S5a, ESI†) correspond to GDY species. These peaks are not distinguished in the spectrum of CF_x.[34,35] X-Ray diffraction (XRD) measurements were employed to identify the composition and phase evolution. XRD data of the CF_x/GDY hybrids (Fig. S5b, ESI†) show that the major structure was unaffected and the GDY nano-walls were ultrathin. Further insights into the chemical compositions and elemental valence of the CF_x and CF_x/GDY hybrids were studied by X-ray photoelectron spectroscopy (XPS) examinations. Compared with C 1s in CF_x (Fig. 2b), the main spectrum of C 1s (Fig. 2c and Fig. S6, ESI†) became wider on account of the conjugated GDY with sp/sp^2 hybrids. The high-resolution C spectrum in CF_x could be divided into four peaks at 284.8 eV (C=C), 286.3 eV (C–C), 290.3 eV covalent (C–F) and 292.1 eV (covalent C–F_2), respectively.[36,37] A new peak at 285.0 eV for the CF_x/GDY hybrids was assigned to C≡C,[19,33,38] and is consistent with the results of the FTIR and Raman spectra. Compared with pure GDY and CF_x (Fig. 2c and d), the C 1s and F 1s XPS spectra of the CF_x/GDY hybrids shifted to higher and lower binding energies, respectively, indicating an apparent electron transfer from GDY to CF_x. The results could be ascribed to the electronic structure modulation of the two-dimensional encapsulated CF_x/GDY hybrids due to the new interaction between electron-rich GDY and CF_x. All the systematic characterizations indicated the form of a two-dimensional encapsulated CF_x/GDY hybrid, which plays an important role in terms of the stability of the complex. Density functional theory (DFT) calculations were performed to investigate the electronic structure of the CF_x/GDY hybrids. As shown in Fig. 2e and f, we could clearly observe the apparent transformation of the total densities of states described for CF_x and CF_x/GDY hybrids. Compared to CF_x with a wide band gap of about 2.6 eV, the introduction of GDY contributed to make the density of states pass through the Fermi level, redistribute the charge of the structure and transform the metallic-like feature, making the bandgap alter. This demonstrated that GDY can improve the electronic conductivity and decrease the charge transfer barrier of CF_x/GDY hybrids. Fig. 2g and h display the electronic density difference of CF_x and CF_x/GDY. The yellow and blue parts represent charge accumulation and depletion, respectively. There was almost no charge transfer among molecules dominated by weak van der Waals forces for CF_x cathodes. However, apparently, the charge accumulation region around CF_x and charge depletion region around GDY were observed, verifying the visibly imbalanced charge distribution, indicating the charge transfer from GDY nanosheets to CF_x particles (Fig. 2i). This confirms the electronic structure modulation of CF_x in CF_x/GDY hybrids, revealing a new interaction forming between GDY and CF_x, which is of benefit to the fast migration of electrons and ions. The electrochemistry performances of cathode CF_x and CF_x/GDY hybrids coupled with lithium metal as the counter electrode were evaluated to verify the superiority of GDY encapsulation and electronic structure modulation. As displayed in Fig. 3a and b, the pristine CF_x material delivered a discharge capacity of

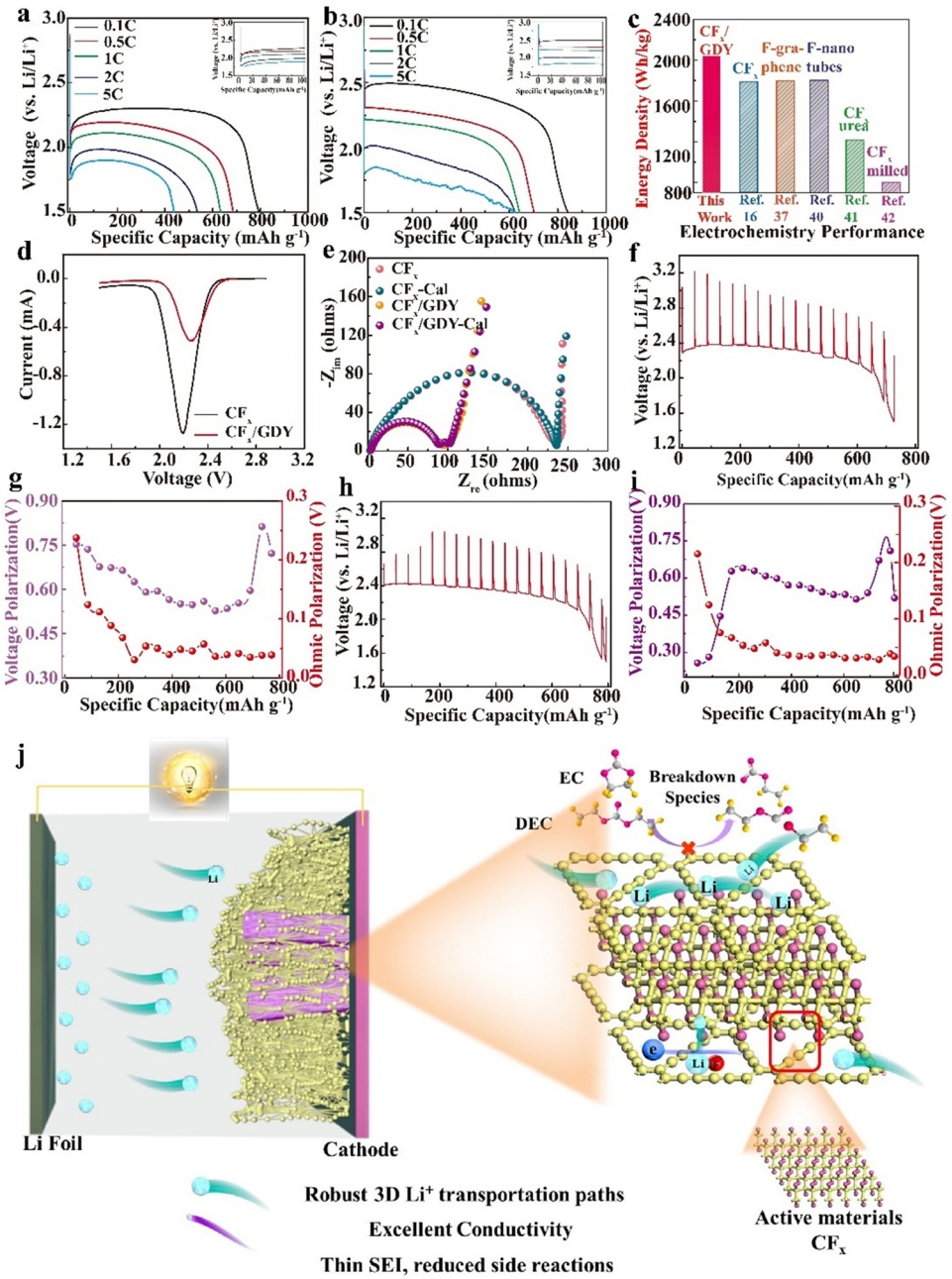

Fig. 3 (a and b) Rate performances of CF_x and CF_x/GDY hybrids. (c) Comparison of energy densities of CF_x/GDY with the reported literature. (d) Cyclic voltammetry profiles and (e) the electrochemistry impedance spectra (EIS). The GITT curves of CF_x (f) and CF_x/GDY hybrids (h) and the related voltage and ohmic polarization curves derived from the GITT plots of various electrodes (g and i). (j) Schematic illustration of the reaction mechanism for CF_x/GDY hybrids.

793.6 mA h g^{-1} at 0.1C and 436.3 mA h g^{-1} at 5C, respectively, while CF_x/GDY hybrids exhibited outstanding rate performances, achieving a specific capacity of 621.6 mA h g^{-1} at 5C. It is worth mentioning that a plateau at ~2.3 V was observed in the curves, indicating a two-phase reaction for CF_x. Interestingly, we could observe a phenomenon that the voltage decreased sharply at the beginning of discharging owing to suffering from a sluggish kinetics process and then gradually increased thanks to the conductive carbon generated during discharge.[39] Unlike CF_x, CF_x/GDY hybrids demonstrated hardly any voltage decay after discharge and a higher voltage plateau. This could be ascribed to the enhanced ion and electronic conductivity. Thus, the CF_x/GDY hybrids provided an energy density as high as 2039.3 W h kg^{-1}, which exceeded the reported energy densities of F-graphene, CF_x, CF_x/urea, and so on (Fig. 3c).[16,37,40–42] The pouch-type electrochemistry performance of CF_x/GDY hybrids is shown in Fig. S7 (ESI†). To gain insight on the electrochemistry behaviours, cyclic voltammetry (CV) was also examined at a sweep rate of 0.1 mV s^{-1}, as shown in Fig. 3d. The CF_x cathode showed a more severe voltage

hysteresis and polarization than those of the CF_x/GDY hybrids, resulting from an enhanced kinetic process. XRD results proved that the peak of CF_x disappear completely and the peaks of LiF and graphitized carbon appeared (Fig. S5c, ESI†) with a reduced I_D/I_G (Fig. S8, ESI†), which certificated that the conversion reaction $CF_x + xLi \rightarrow C + xLiF$ happened during the discharge process. Moreover, electrical impedance spectra (EIS) were carried out and fitted to an R(QR)(QR)(CR) equivalent-circuit model (Fig. 3e, Fig. S9, and Table S1, ESI†).[41,42] CF_x/GDY hybrids showed a smaller radius of the semicircle in a high frequency range, responding to a charge transfer resistance between the electrolyte and cathode[43–45] compared to that of pristine CF_x after discharge, explaining the faster reaction kinetics process and greatly enhanced electrochemistry performance (Fig. 3e). To further assess the effective effects brought about by two-dimensional layered encapsulation, GITT was employed to analyse the kinetics behaviours of CF_x/GDY. Fig. 3f and h correspond to the GITT curves of the CF_x and CF_x/GDY hybrids, respectively. In contrast to CF_x (Fig. 3g), CF_x/GDY hybrids could effectively minify the voltage polarization and ohmic polarization revealed by GITT (Fig. 3i). These results clearly confirmed that the GDY nano-walls on the interface could enhance conductivity and Li^+ diffusion, resulting in a reduced polarization and accelerated dynamics behaviour,[46,47] consistent with the conclusion arrived at through the EIS curves. As displayed in Fig. 3j, the CF_x/GDY hybrids could inhabit interface side reactions, accelerate electronic charge transfer and remain in a robust 3D lithium-ion transport channel. In addition, the two-dimensional encapsulation method could adjust the electronic characteristics of CF_x/GDY hybrids and change the interfacial contact between electrode and electrolyte stemming from the binding between CF_x and GDY, enabling a superior electrochemistry performance.

Further characterization analyses were done to get a comprehensive understanding of the reason for the brilliant electrochemistry performance of the CF_x/GDY hybrids. XPS methods were carried out to detect the compositions and valence change of samples after cycling. In contrast to the C 1s peak on CF_x (Fig. 4a), we could observe the absence of C═O–C and the existence of weak C–O and C═O in intensity on the CF_x/GDY hybrids, which stemmed from the decomposition of the electrolyte (Fig. 4b).[36,48] Besides, the existence of C≡C verified the solidity of the two-dimensional layered GDY encapsulation. We also detected that the composition and content of the CF_x and CF_x/GDY hybrids could alter on the externality after 30 s and 60 s of etching by Ar^+ ions. The C–O, C═O and C═O–C could be observed at different depth for CF_x with only a small surface area for the CF_x/GDY hybrids (Fig. 4c). The disappearance of C═O in CF_x/GDY hybrids with etching for 30 s and 60 s indicated a thin SEI layer after discharging. Combined with the weakened peak intensity of the F signals (Fig. 4e)[49,50] when compared with those of CF_x in Fig. 4d, the intensities of C–F/$LiPO_xF_y$ and LiF were greatly reduced and no related signals of them were observed after etching for 30 s and 60 s, which revealed the effectively suppressed decomposition of the electrolyte on the CF_x/GDY hybrids. It can be concluded

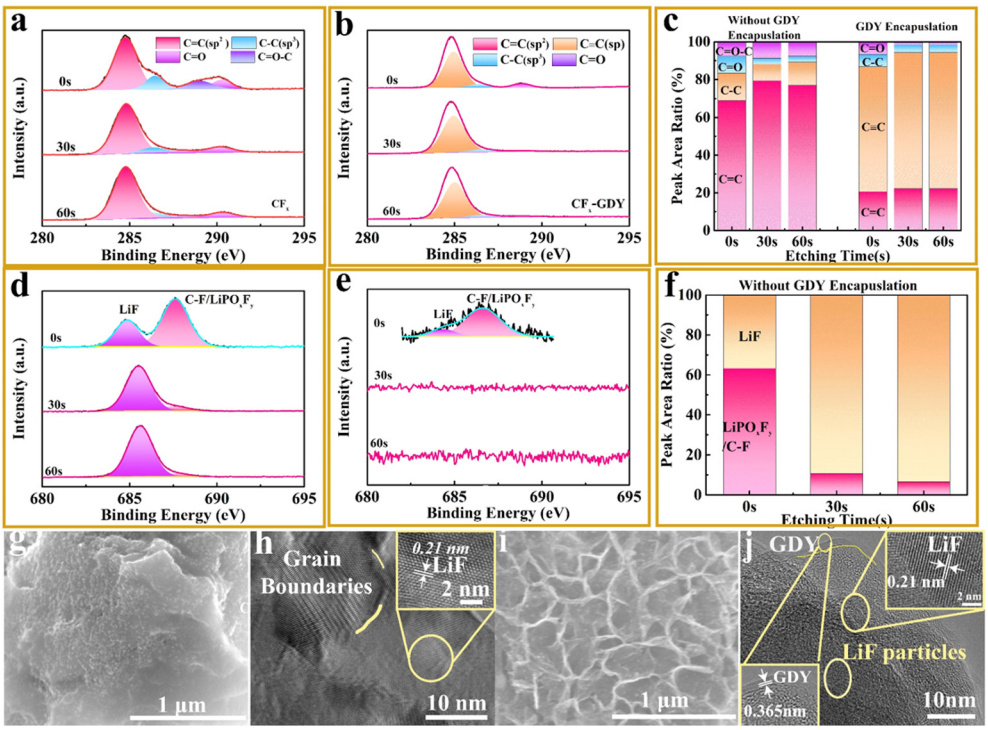

Fig. 4 C XPS spectra (a and b), F spectra (d and e) and the relative contents (c and f) stemming from the different depths given in Fig. (a and b) and (d and e) of CF_x and CF_x/GDY hybrids at the discharge state of 1.5 V, respectively. The SEM images (g and i) and HRTEM images (h and j) of CF_x and CF_x/GDY hybrids, respectively.

that the GDY encapsulation is capable of altering the interfacial characteristics between the electrode and electrolyte, thus making the contact close upon cycling. A thick SEI layer that formed on the CF_x could be noticed after discharging (Fig. 4g). On the contrary, hardly any LiF particles (Fig. 4i) could be observed on the surface of the CF_x/GDY hybrids because the two-dimensional encapsulation with variable interface properties could hinder the diffusion of element F and the conformation of LiF on the surface, maintaining the 3D lithium-ion intercalation channel. Besides, we learned that the amount of element O related to the reduction of electrolyte on the surface of CF_x/GDY hybrids was reduced (Fig. S10a and b, ESI†).

At the end of discharge, the accumulation of LiF particles with highly crystalline and grain boundaries could be observed (Fig. 4h and Fig. S11a, ESI†). On the contrary, LiF nanoparticles were dispersed and the 3D GDY framework was maintained on the surface of the CF_x/GDY hybrids as displayed in Fig. 4k and Fig. S11b (ESI†), respectively. This revealed that the decomposition of the electrolyte was detrimental to the electrochemistry performance. The sum of the above analysis demonstrates that the two-dimensional layered encapsulated CF_x/GDY hybrids inhibited the degradation of the electrolyte and produced LiF on the exterior of cathode, leading the interfacial impedance to diminish and to an improvement in the ion and electron transfer. To investigate the chemical compositions and crystalline structure evolution, we implemented *ex situ* XRD to evaluate the products at different depths of discharge. We chose the different depths of discharge for CF_x (Fig. S12a, ESI†) and the CF_x/GDY hybrids (Fig. S12c, ESI†) to discuss the phase evolution during the discharge process. As displayed in Fig. S12b (ESI†), we could observe that the CF_x maintained its crystalline structure in the early reaction stage, and the discharge products graphite and LiF could be observed when the depth of discharge was up to 10%. The peak intensity of CF_x weakened with increasing depth of discharge (DOD) and almost disappeared completely when the DOD was over 80%. At the end of discharge, we could only detect graphite and LiF, indicating the complete conversion reaction of CF_x. In addition, we detected no intermediate phase in our experiments. We could not notice any apparent differences for CF_x and CF_x/GDY during the discharge process (Fig. S12d, ESI†). In short, the two-dimensional GDY encapsulation has no major impact on the phase evolution of CF_x.

Conclusions

In summary, we have demonstrated an effective and convenient fabrication strategy to form two-dimensional layered encapsulated CF_x electrodes to address the theme of inferior conductivity. The CF_x/GDY hybrids exhibited an excellent specific capacity and outstanding rate performances for LPBs. With the benefit of a 3D conductive network and controllable voids, the discharge voltage and energy density were significantly enhanced. In particular, the CF_x/GDY hybrids exhibited a specific capacity of 621.6 mA h g^{-1} at 5C, exceeding the specific capacity of CF_x. Theoretical calculation and experimental research demonstrated that GDY encapsulation could modulate the electronic structure and strengthen the contact among particles of the CF_x/GDY hybrids, providing a facile and convenient 3D ion diffusion and electronic transfer. Meanwhile, the GDY nano-walls are capable of hindering a direct contact between CF_x and the electrolyte to transform the interface, bringing about a reduced impedance and an optimized lithium-ion intercalation process. Our findings highlight the GDY nanosheets as a potential compound to modulate the structure and achieve a two-dimensional encapsulation appropriate for high-performance lithium-ion batteries, while also opening a path to achieve a commercialized application in some fields to some extent.

Experimental section

Material preparation

Fluorinated graphite CF_x was purchased from Shanghai Chemical Technology Co., Ltd, China, and used as received without further purification. Briefly, the CF_x powder supported by copper foil was immersed in a mixed solution of 2 mg of HEB, 1 mL of pyridine, and 10 mL of diethyl ether in a sealed glass vessel. After reaction at room temperature for two days, the GDY nanosheets successfully covered the CF_x sample. Heat treatment at 180 °C was necessary and critical to remove any residues and moisture for the following characterization and electrochemistry performance.

Characterizations

The crystal structures of CF_x and CF_x/GDY were examined through using an X-ray diffractometer equipped with a Cu Kα radiation source (λ_1 = 1.54060 Å) at a voltage of 40 kV and a current of 30 A. We measured the diffraction angle (2θ) between 5 °C and 90 °C. The morphology and particle size of the synthesized samples were collected by a field emission scanning electron microscope (S-4800, 10 kV) and a field emission transmission electron microscope (JEOL-2100F, 200 KV) attached to an energy dispersive X-ray spectrometer (EDS). Element composition and valence state analysis were conducted by X-ray photoelectron spectroscopy (XPS). Cyclic voltammetry (CV) and electrochemistry impedance spectroscopy (EIS) were used to explain the differences between CF_x and CF_x/GDY with the assistance of an Autolab PG302N electrochemical workstation.

Electrochemistry measurements

For the electrochemistry performance, a mixture of the active materials, acetylene black (Super-P), poly(vinyl difluoride) (PVDF, Aldrich) at a weight ratio of 8 : 1 : 1 and the proper amount of a *N*-methyl pyrrolidone (NMP) solvent was added and then deposited on a pure Al foil (99%, Goodfellow). Before dividing the coating Al foil into circular electrodes, it was necessary to dry it in a vacuum oven at 80 °C for 10 h. The electrochemistry performances, including rate performance

and charge–discharge curves, were performed by assembling CR2032 coin cells in an argon-filled glove box. Lithium metal was used as counter electrode and a polypropylene membrane was utilized as the separator. The electrolyte was 1 M $LiPF_6$ in ethylene carbonate (EC)/dimethyl carbonate (DMC)/diethyl carbonate (DEC) (1 : 1 : 1 vol%). Galvanostatic tests within a window voltage of 1.5–3.5 V were adapted to the new assembled coin cells and were tested on a Land CT2001A battery test system.

Author contributions

Conceptualization: Yuliang Li conceived and designed the research, and reviewed and edited the manuscript. Jingchi Gao synthesized the cathode and carried out a series of characterizations to analyse the results. Feng He conducted the theoretical calculations. Changshui Huang assisted with the data analysis, and organized and wrote the paper. Yurui Xue and Zicheng Zuo gave useful help.

Conflicts of interest

There are no conflicts to declare.

Acknowledgements

This work was supported by the National Nature Science Foundation of China (21790050, 21790051), the National Key Research and Development Project of China (2018YFA0703501), and the Key Program of the Chinese Academy of Sciences (QYZDY-SSW-SLH015).

References

1 J. L. Shi, D. D. Xiao, M. Ge, X. Yu, Y. Chu, X. Huang, X. D. Zhang, Y. X. Yin, X. Q. Yang, Y. G. Guo, L. Gu and L. J. Wan, *Adv. Mater.*, 2018, **30**, 1705575.
2 H. Park, H.-D. Lim, H.-K. Lim, W. M. Seong, S. Moon, Y. Ko, B. Lee, Y. Bae, H. Kim and K. Kang, *Nat. Commun.*, 2017, **8**, 14989.
3 M. Jo, M. Noh, P. Oh, Y. Kim and J. Cho, *Adv. Energy Mater.*, 2014, **4**, 1301583.
4 Y. K. Sun, S. T. Myung, B. C. Park, J. Prakash, I. Belharouak and K. Amine, *Nat. Mater.*, 2009, **8**, 320–324.
5 L. Wang, Z. Wu, J. Zou, P. Gao, X. Niu, H. Li and L. Chen, *Joule*, 2019, **3**, 2086–2102.
6 E. Rangasamy, J. Li, G. Sahu, N. Dudney and C. Liang, *J. Am. Chem. Soc.*, 2014, **136**, 6874–6877.
7 C. A. Vincent, *Solid State Ionics*, 2000, **134**, 241–267.
8 Y. Dai, Y. Fang, S. Cai, L. Wu, W. Yang, H. Yan, J. Xie, J.-C. Zheng, E. Takeuchi and Y. Zhu, *J. Electrochem. Soc.*, 2017, **162**, A1–A7.
9 F. O. H. Touhara, *Carbon*, 2000, **38**, 241–267.
10 D. O'Hagan, *Chem. Soc. Rev.*, 2008, **37**, 308–319.
11 Z. Ding, C. Yang, J. Zou, S. Chen, K. Qu, X. Ma, J. Zhang, J. Lu, W. Wei, P. Gao and L. Wang, *Adv. Mater.*, 2020, e2006118.
12 Q. Zhang, S. D'Astorg, P. Xiao, X. Zhang and L. Lu, *J. Power Sources*, 2010, **195**, 2914–2917.
13 H. Groult, C. M. Julien, A. Bahloul, S. Leclerc, E. Briot and A. Mauger, *Electrochem. Commun.*, 2011, **13**, 1074–1076.
14 G.-L. Xu, Q. Liu, K. K. S. Lau, Y. Liu, X. Liu, H. Gao, X. Zhou, M. Zhuang, Y. Ren, J. Li, M. Shao, M. Ouyang, F. Pan, Z. Chen, K. Amine and G. Chen, *Nat. Energy*, 2019, **4**, 484–494.
15 P. Meduri, H. Chen, X. Chen, J. Xiao, M. E. Gross, T. J. Carlson, J.-G. Zhang and Z. D. Deng, *Electrochem. Commun.*, 2011, 1344–1348.
16 C. Jiang, B. Wang, Z. Wu, J. Qiu, Z. Ding, J. Zou, S. Chen, P. Gao, X. Niu, L. Wang and H. Li, *Nano Energy*, 2020, **70**, 104552.
17 G. Li, Y. Li, H. Liu, Y. Guo, Y. Li and D. Zhu, *Chem. Commun.*, 2010, **46**, 3256–3258.
18 H. Shang, Z. Zuo, L. Yu, F. Wang, F. He and Y. Li, *Adv. Mater.*, 2018, **30**, e1801459.
19 F. Wang, Z. Zuo, L. Li, F. He, F. Lu and Y. Li, *Adv. Mater.*, 2019, **31**, e1806272.
20 J. He, N. Wang, Z. Cui, H. Du, L. Fu, C. Huang, Z. Yang, X. Shen, Y. Yi, Z. Tu and Y. Li, *Nat. Commun.*, 2017, **8**, 1172.
21 X. Gao, Z. Zuo, F. Wang, Q. Chang, H. Pan, L. Li, F. He and Y. Li, *Energy Storage Mater.*, 2022, **45**, 110–118.
22 L. Li, Z. Zuo, H. Shang, F. Wang and Y. Li, *Nano Energy*, 2018, **53**, 135–143.
23 C. Xie, X. Hu, Z. Guan, X. Li, F. Zhao, Y. Song, Y. Li, X. Li, N. Wang and C. Huang, *Angew. Chem., Int. Ed.*, 2020, **59**, 13542–13546.
24 N. Wang, J. He, Z. Tu, Z. Yang, F. Zhao, X. Li, C. Huang, K. Wang, T. Jiu, Y. Yi and Y. Li, *Angew. Chem., Int. Ed.*, 2017, **56**, 10740–10745.
25 L. Li, Z. Zuo, F. Wang, J. Gao, A. Cao, F. He and Y. Li, *Adv. Mater.*, 2020, **32**, e2000140.
26 Y. Du, W. Zhou, J. Gao, X. Pan and Y. Li, *Acc. Chem. Res.*, 2020, **53**, 459–469.
27 J. He, N. Wang, Z. Yang, X. Shen, K. Wang, C. Huang, Y. Yi, Z. Tu and Y. Li, *Energy Environ. Sci.*, 2018, **11**, 2893–2903.
28 J. He, T. Lu, K. Wang, X. Wang, X. Li, X. Shen, J. Gao, W. Si, Z. Yang and C. Huang, *Adv. Funct. Mater.*, 2020, 2005933.
29 Y. Yi, J. Li, W. Zhao, Z. Zeng, C. Lu, H. Ren, J. Sun, J. Zhang and Z. Liu, *Adv. Funct. Mater.*, 2020, **30**, 2003039.
30 N. Wang, X. Li, Z. Tu, F. Zhao, J. He, Z. Guan, C. Huang, Y. Yi and Y. Li, *Angew. Chem., Int. Ed.*, 2018, **57**, 3968–3973.
31 C. Huang, S. Zhang, H. Liu, Y. Li, G. Cui and Y. Li, *Nano Energy*, 2015, **11**, 481–489.
32 L. Hui, Y. Xue, B. Huang, H. Yu, C. Zhang, D. Zhang, D. Jia, Y. Zhao, Y. Li, H. Liu and Y. Li, *Nat. Commun.*, 2018, **9**, 5309.
33 Y. Xue, Y. Guo, Y. Yi, Y. Li, H. Liu, D. Li, W. Yang and Y. Li, *Nano Energy*, 2016, **30**, 858–866.
34 L. Hui, Y. Xue, F. He, D. Jia and Y. Li, *Nano Energy*, 2019, **55**, 135–142.
35 J. Zhou, X. Gao, R. Liu, Z. Xie, J. Yang, S. Zhang, G. Zhang, H. Liu, Y. Li, J. Zhang and Z. Liu, *J. Am. Chem. Soc.*, 2015, **137**, 7596–7599.

36 Q. Li, W. Xue, X. Sun, X. Yu, H. Li and L. Chen, *Energy Storage Mater.*, 2021, **38**, 482–488.
37 C. Sun, Y. Feng, Y. Li, C. Qin, Q. Zhang and W. Feng, *Nanoscale*, 2014, **6**, 2634–2641.
38 W. Zhou, H. Shen, C. Wu, Z. Tu, F. He, Y. Gu, Y. Xue, Y. Zhao, Y. Yi, Y. Li and Y. Li, *J. Am. Chem. Soc.*, 2019, **141**, 48–52.
39 C. Peng, Y. Li, F. Yao, H. Fu, R. Zhou, Y. Feng and W. Feng, *Carbon*, 2019, **153**, 783–791.
40 Y. Li, X. Wu, C. Liu, S. Wang, P. Zhou, T. Zhou, Z. Miao, W. Xing, S. Zhuo and J. Zhou, *J. Mater. Chem.*, 2019, **A7**, 7128–7137.
41 P. Zhou, J. Weng, X. Liu, Y. Li, L. Wang, X. Wu, T. Zhou, J. Zhou and S. Zhuo, *J. Power Sources*, 2019, **414**, 210–217.
42 M. A. Reddy, B. Breitung and M. Fichtner, *ACS Appl. Mater. Interfaces*, 2013, **5**, 11207–11211.
43 S.-K. Jung, H. Gwon, J. Hong, K.-Y. Park, D.-H. Seo, H. Kim, J. Hyun, W. Yang and K. Kang, *Adv. Energy Mater.*, 2014, **4**, 1300787.
44 W. Lee, S. Muhammad, T. Kim, H. Kim, E. Lee, M. Jeong, S. Son, J.-H. Ryou and W.-S. Yoon, *Adv. Energy Mater.*, 2018, **8**, 1701788.
45 W. Liu, X. Li, D. Xiong, Y. Hao, J. Li, H. Kou, B. Yan, D. Li, S. Lu, A. Koo, K. Adair and X. Sun, *Nano Energy*, 2018, **44**, 111–120.
46 J. Y. Liang, X. X. Zeng, X. D. Zhang, P. F. Wang, J. Y. Ma, Y. X. Yin, X. W. Wu, Y. G. Guo and L. J. Wan, *J. Am. Chem. Soc.*, 2018, **140**, 6767–6770.
47 M. Yoon, Y. Dong, J. Hwang, J. Sung, H. Cha, K. Ahn, Y. Huang, S. J. Kang, J. Li and J. Cho, *Nat. Energy*, 2021, **6**, 362–371.
48 X. L. Wangda Li, H. Celio, P. Smith, A. Dolocan, M. Chi and A. Manthiram, *Adv. Energy Mater.*, 2018, **8**, 1703154.
49 Y. Zhu, L. Zhang, H. Zhao and Y. Fu, *J. Mater. Chem.*, 2017, **A5**, 796–803.
50 X. D. Zhang, J. L. Shi, J. Y. Liang, Y. X. Yin, J. N. Zhang, X. Q. Yu and Y. G. Guo, *Adv. Mater.*, 2018, e1801751.